Distinguishing free and anomalous diffusion by rectangular fluorescence recovery after photobleaching: a Monte Carlo study

Ben De Clercq
Bart Cleuren
Hendrik Deschout
Kevin Braeckmans
Marcel Ameloot

Distinguishing free and anomalous diffusion by rectangular fluorescence recovery after photobleaching: a Monte Carlo study

Ben De Clercq,[a] **Bart Cleuren,**[b] **Hendrik Deschout,**[c] **Kevin Braeckmans,**[c] **and Marcel Ameloot**[a]
[a]Hasselt University, Biomedical Research Institute, Agoralaan Building C, B-3590 Diepenbeek, Belgium
[b]Hasselt University, Theoretical Physics, Agoralaan Building D, B-3590 Diepenbeek, Belgium
[c]Ghent University, Biophotonic Imaging Group, Laboratory of General Biochemistry and Physical Pharmacy, Harelbekestraat 72, B-9000 Gent, Belgium

Abstract. Fluorescence recovery after photobleaching (FRAP) is a common technique to probe mobility of fluorescently labeled proteins in biological membranes by monitoring the time-dependence of the spatially integrated fluorescence signals after a bleaching pulse. Discrimination by FRAP between free diffusion with an immobile fraction (FDIM) and the phenomenological model for anomalous diffusion based on the time-dependent diffusion coefficient (TDDC) is a challenging problem, requiring extremely long observation times for differentiation. Recently, rectangular FRAP (rFRAP) has been introduced for normal diffusion by considering not only the temporal but also spatial information, taking the effective point spread function of the optical system into account. In this work we provide an extension of rFRAP toward anomalous diffusion according to the continuous time random walk (CTRW). We explore whether the spatial information in rFRAP allows for enhanced discrimination between FDIM, TDDC, and CTRW in a single experiment within a feasible time window. Simulations indicate that rFRAP can indeed differentiate the different models by evaluating the spatial autocorrelation of the differences between the measured and fitted pixel values. Hence, rFRAP offers a tool that is capable of discriminating different types of diffusion at shorter time scales than in the case where spatial information is discarded. © *2013 Society of Photo-Optical Instrumentation Engineers (SPIE)* [DOI: 10.1117/1.JBO.18.7.076012]

Keywords: fluorescence recovery after photobleaching; anomalous diffusion; continuous time random walk; simulation; model discrimination.

Paper 130380R received May 30, 2013; revised manuscript received Jun. 9, 2013; accepted for publication Jun. 11, 2013; published online Jul. 10, 2013.

1 Introduction

The vital protein movement in biological cells, and particularly in the membrane, is mainly diffusion driven.[1,2] Because of the highly heterogeneous nature of the plasma membrane, both in composition and structure, transmembrane proteins are unlikely to exhibit normal diffusion.[3,4] This means that the mean square displacement (MSD) does not evolve linearly in time t as for normal diffusion, but is usually modeled as MSD $\propto t^\alpha$, with α the so-called anomalous exponent. In the case of hindered or anomalous subdiffusion, $0 < \alpha < 1$. Normal and hindered diffusion can be simulated by means of continuous time random walk (CTRW).[5]

Several microfluorimetric methods are utilized to explore the diffusive behavior of particles and proteins. Both single particle and ensemble-oriented approaches are used.[6–9] In this paper the focus is on fluorescence recovery after photobleaching (FRAP)[10–12] as this method is readily available in many laboratories.[13–15] FRAP is an ensemble-oriented technique based on photobleaching a significant amount of fluorescent labels within a certain region of interest (ROI).[16] Because of diffusion, the proteins with unbleached labels from the surroundings will exchange with the proteins with bleached labels in the ROI. The resulting recovery of the fluorescence signal is recorded under attenuated excitation. The diffusion is related to the rate at which the fluorescence recovers.

Various analysis models are available when the experimental FRAP data cannot be described by purely free diffusion. In this work we consider (1) free diffusion in combination with an immobile fraction (FDIM), (2) a time-dependent diffusion coefficient (TDDC),[17,18] and (3) CTRW to incorporate anomalous diffusion.[19]

In FDIM, the mobile fraction of the proteins within the ROI is determined by comparing the fluorescence intensity after a sufficiently long recovery time to the prebleach intensity. The TDDC and CTRW approaches are discussed in more detail in the following sections. Briefly, in TDDC a time-dependent diffusion coefficient, mimicking MSD $\propto t^\alpha$, is considered in the normal diffusion equation. However, the physical basis of this phenomenological model is not clear.[20] Instead, the CTRW model provides a physically justified basis by assuming that the diffusing particle moves along traps with a residence time distribution according to a power law.[5,19,21]

Recognizing anomalous diffusion and discriminating different models remains a challenge. FDIM can mask the effects of long tail kinetics and misleading results can be obtained.[22] Anomalous subdiffusion is an example of such long tail kinetics. It has been suggested that an FRAP measurement over five time decades is needed to unambiguously distinguish FDIM and

TDDC.[17] Alternatively, FRAP experiments can be conducted at various ROI sizes. In the case of anomalous diffusion, the estimated apparent mobile fraction in FDIM will show a dependence on the ROI size.[23,24]

Originally, the bleaching in an FRAP experiment was achieved with an intense, stationary laser beam, yielding a Gaussian-shaped bleached profile.[10] ROIs with different widths can be obtained by using different objectives.[25] Due to the introduction of the confocal laser-scanning microscope (CLSM), a wide variety of geometries can be bleached.[26–29] The recovery curve is then built from the time sequence of the spatially integrated images of the ROI.

When using a CLSM, a rectangular ROI is more natural because of the inherent scanning procedure. Closed expressions for data analysis are available.[29] However, rectangular ROIs are less commonly used, although they offer some advantages over circular ROIs. The observed ROI is not required to match the bleached ROI and can differ in length and width, allowing minimization of the artifacts that originate from the curvature in a membrane.[29] Dushek et al.[29] have derived a closed analytical expression for rectangular ROIs that offers the possibility to combine spatial and time information, whereas for circular ROIs such a closed formula is not available.[30] Later on, Deschout et al.[31] showed that retaining the spatial information offers the possibility to take into account the effects of the finite size of the focused laser beam without additional measurements.

The aim of this work is to explore the discrimination power between various models with rFRAP when both time and spatial information are considered, i.e., when the full-intensity profile is taken into account. To this end, simulations of FDIM and of anomalous subdiffusion are performed. Comparison with the spatially integrated approach is carried out.

2 Simulating Free and Anomalous Diffusion

Simulations of free and anomalous diffusions are performed according to the CTRW implementation introduced by Lubelski and Klafter.[21] Particles move on a two-dimensional square grid (mesh size r_0) by jumping randomly to one of the four neighboring positions. The time between two consecutive jumps, the so-called waiting time, is randomly distributed according to the waiting time probability density function (pdf), $\Psi(t)$. This pdf is defined such that the probability for the particle to jump between time t and $t + dt$ is given by $\Psi(t)dt$. The properties of the particle motion strongly depend on this waiting time pdf. If the first moment exists, i.e., when the average waiting time is finite, the system shows normal diffusion[19] and is described by Fick's second law.

$$\frac{\partial C(x, y, t)}{\partial t} = D\nabla^2 C(x, y, t), \qquad (1)$$

where C is the concentration of particles as a function of spatial variables, x and y, and time, t. D is the diffusion coefficient and ∇^2 is the two-dimensional Laplace operator. Free diffusion is simulated by means of exponentially distributed waiting times. The diffusion coefficient D is related to the jump length r_0 and the average waiting time τ by

$$D = r_0^2/4\tau. \qquad (2)$$

If on the other hand the waiting time pdf does not have a finite first moment, the system will exhibit anomalous subdiffusion.[19] In the simulations, the waiting time pdf is obtained

by taking the time derivative of the Mittag-Leffler function, E_α.[21]

$$E_\alpha[-(t/\tau)^\alpha] = \sum_{n=0}^{\infty} \frac{[-(t/\tau)^\alpha]^n}{\Gamma(n\alpha + 1)}, \qquad (3)$$

$$\Psi(t) = -\frac{d}{dt} E_\alpha[-(t/\tau)^\alpha], \qquad (4)$$

where Γ is the gamma-function and τ is a time scaling factor. Normal diffusion is obtained by setting $\alpha = 1$, yielding an exponential pdf and a finite average waiting time equal to τ. Setting $\alpha < 1$ leads to anomalous subdiffusion. This process is no longer described by Fick's law [Eq. (1)], but rather by the so-called fractional diffusion equation, also known as the fractional Fokker–Planck equation.[21]

$$\frac{\partial C_\alpha(x, y, t)}{\partial t} = \frac{1}{\Gamma(\alpha)} \frac{\partial}{\partial t} \int_0^t (t - s)^{\alpha-1} K_\alpha \nabla^2 C_\alpha(x, y, s) ds,$$
$$\qquad (5)$$

where C_α denotes the concentration and K_α is the transport factor. K_α is related to the time scaling factor, τ, and the elementary jump length, r_0, by

$$K_\alpha = r_0^2/4\tau^\alpha. \qquad (6)$$

The solution $C_\alpha(x, y, t)$ of the fractional diffusion equation [Eq. (5)] is related to the solution for free diffusion [Eq. (1)], $C(x, y, t)$, by[21]
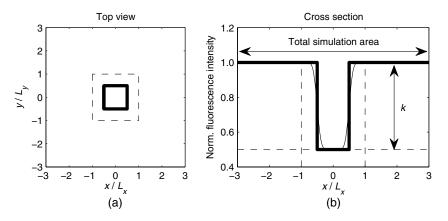
$$C_\alpha(x, y, t) = \int_0^\infty A(s, t) C(x, y, s*) ds, \qquad (7)$$

where $s* = K_\alpha s/D$ and $A(s, t)$ is the modified one-sided Levy distribution function. Replacing the argument t in $C(x, y, t)$ by $s*$ is equivalent to replacing Dt in the expression for $C(x, y, t)$ by $K_\alpha s$. For general α, the modified one-sided Levy distribution function is given by the series expansion

$$A(s, t) = \frac{1}{s} \sum_{n=0}^{\infty} \frac{(-1)^n}{\Gamma(1 - \alpha - n\alpha)\Gamma(1 + n)} \left(\frac{s}{t^\alpha}\right)^{1+n}. \qquad (8)$$

3 Data Analysis

The simulated FRAP data are analyzed in two different ways. In the first approach, common FRAP curves are obtained by integrating the intensity profile over the nominally bleached ROI, i.e., the user-defined region ($L_x \times L_y$; Fig. 1). The second approach is based on fitting the time evolution of the spatial intensity profile directly. In this case, a larger ROI than the nominally bleached ROI is taken into account ($2L_x \times 2L_y$; Fig. 1). Hence, the recovery inside the ROI as well as the fluorescence changes outside the ROI are considered. FRAP curves and intensity profiles are fitted with three different diffusion models as discussed below. The functions given below assume that the data are normalized with respect to their prebleach values.

Fig. 1 Top view (a) and cross-section of the bleached ROI along $y = 0$ (b). The distances x and y are normalized with respect to the size of the nominally bleached ROI, L_x and L_y. The thick solid line indicates the nominally bleached profile. This is the area over which the intensity is integrated when FRAP curves are fitted. The area of the analyzed ROI, when the intensity profile is fitted, measures four times the area of the nominally bleached ROI (dashed lines in the left panel). The thin solid line in the right panel shows the effectively bleached ROI, illustrating the effect of the bleaching and imaging PSF. The horizontal dashed line indicates the bleaching depth k. The total simulation area is at least 36 times the area of the nominally bleached ROI.

3.1 Free Diffusion with a Mobile Fraction (Model FDIM)

In the case of free diffusion, the MSD evolves linearly in time.

$$\text{MSD} = 4Dt. \tag{9}$$

The intensity profile as a function of time during recovery, $F(x, y, t)$, is given by[31]

$$
F(x, y, t) = 1 - \frac{k}{4}\left[\text{erf}\left(\frac{x + L_x/2}{\sqrt{4Dt + r^2}}\right)\right.
$$
$$
\left. - \text{erf}\left(\frac{x - L_x/2}{\sqrt{4Dt + r^2}}\right)\right]\left[\text{erf}\left(\frac{y + L_y/2}{\sqrt{4Dt + r^2}}\right)\right.
$$
$$
\left. - \text{erf}\left(\frac{y - L_y/2}{\sqrt{4Dt + r^2}}\right)\right], \tag{10}
$$

where erf is the error function, k is the bleaching depth (Fig. 1), L_x and L_y are the sizes of the nominally bleached rectangle [the center of the rectangle has coordinates $(0, 0)$], t is the time since bleaching, and r is the resolution parameter. This parameter accounts for the finite resolution during bleaching and acquisition of the recovery images. It is defined as $r^2 = (r_{im}^2 + r_b^2)/2$, where r_b and r_{im} are the respective half-width waists at e^{-2} of the effective bleaching and imaging point spread function (PSF). Integrating the intensity profile over the nominally bleached area yields the recovery curve, denoted by F_{int}:

$$
F_{int}(t) = \int_{-L_y/2}^{L_y/2}\int_{-L_x/2}^{L_x/2} F(x, y, t)\mathrm{d}x\mathrm{d}y
$$
$$
= 1 - \frac{k}{L_x L_y}\times\left\{L_x\text{erf}\left(\frac{L_x}{\sqrt{4Dt + r^2}}\right) + \sqrt{\frac{4Dt + r^2}{\pi}}\right.
$$
$$
\times\left[\exp\left(-\frac{L_x^2}{4Dt + r^2}\right) - 1\right]\right\}\times\left\{L_y\text{erf}\left(\frac{L_y}{\sqrt{4Dt + r^2}}\right)\right.
$$
$$
\left. + \sqrt{\frac{4Dt + r^2}{\pi}}\left[\exp\left(-\frac{L_y^2}{4Dt + r^2}\right) - 1\right]\right\}. \tag{11}
$$

Apart from the introduction of the resolution parameter r, Eq. (11) is a simplified form of the formula previously published by Dushek and Coombs,[29] for the particular case that the integration area equals the nominally bleached ROI. Equations (10) and (11) can be extended for the case that some molecules are essentially fixed on the time scale of the experiment. The mobile fraction, M, for both the integrated FRAP curve and the intensity profile, is introduced as

$$F_M(x, y, t) = MF(x, y, t) - (1 - M)F(x, y, 0), \tag{12}$$

$$F_{int,M}(t) = MF_{int}(t) - (1 - M)F_{int}(0), \tag{13}$$

with $F(x, y, 0)$ and $F(0)$ the fluorescence intensity immediately after the bleaching step.

3.2 Anomalous Diffusion: Physical Approach (Model CTRW)

When anomalous diffusion is modeled according to CTRW, the MSD as function of time is given by[21]

$$\text{MSD} = \frac{4K_\alpha t^\alpha}{\Gamma(1 + \alpha)}. \tag{14}$$

Note that for $\alpha = 1$, Eq. (9) is essentially retrieved. The expressions for the intensity profile and the integrated FRAP curves can be derived by applying the same transformation as is done for the solution of the diffusion equation [Eq. (7)]. The intensity profile in the images, considering the finite resolution, during recovery, $F(x, y, t)$, is given by

$$F(x, y, t) = L(x, y) \otimes \text{PSF}_b(x, y) \otimes C_\alpha(x, y, t)$$
$$\otimes \text{PSF}_{im}(x, y), \tag{15}$$

where $\otimes$ denotes the two-dimensional spatial convolution product, L is the ideal ROI normalized by the prebleach intensity, PSF_b is the bleaching PSF, and PSF_{im} is the imaging PSF. This can be rewritten as

$$F_\alpha(x, y, t) = F(x, y, 0) \otimes C_\alpha(x, y, t) = F(x, y, 0)$$
$$\otimes \int_0^\infty A(s, t)C(x, y, s*)\mathrm{d}s, \qquad (16)$$

$$F_\alpha(x, y, t) = \int_0^\infty A(s, t)[F(x, y, 0) \otimes C(x, y, s*)]\mathrm{d}s$$
$$= \int_0^\infty A(s, t)F(x, y, s*)\mathrm{d}s. \qquad (17)$$

The integrated FRAP curve, $F_{int,\alpha}(t)$, is given by

$$F_{int,\alpha}(t) = \int_{-L_y/2}^{L_y/2} \int_{-L_x/2}^{L_x/2} \int_0^\infty A(s, t)F(x, y, s*)\mathrm{d}s\mathrm{d}x\mathrm{d}y. \qquad (18)$$

This can be rewritten as

$$F_{int,\alpha}(t) = \int_0^\infty A(s, t) \int_{-L_y/2}^{L_y/2} \int_{-L_x/2}^{L_x/2} F(x, y, s*)\mathrm{d}x\mathrm{d}y\mathrm{d}s$$
$$= \int_0^\infty A(s, t)F_{int}(s*)\mathrm{d}s. \qquad (19)$$

In the remainder of this work, this anomalous diffusion model will be referred to as CTRW model.

3.3 Anomalous Diffusion: Phenomenological Approach (Model TDDC)

In contrast to the CTRW model, the TDDC is based on a phenomenological approach.[17,18] In this case the MSD is given by[32]

$$\mathrm{MSD} = \frac{4K_\alpha*}{\alpha}t^\alpha. \qquad (20)$$

The expressions for TDDC are obtained in a straightforward way by formally substituting the factor Dt in the formulas for normal diffusion [Eqs. (10) and (11)] by $K_\alpha * t^\alpha/\alpha$.

4 Experimental Procedures

4.1 Simulation Procedure

A priority queue obtained by arranging the waiting times to the next jumps in ascending order is used to determine which particle is the next to make a jump. This particle jumps to one of the four nearest neighboring grid points, chosen at random, and is given a new random waiting time before being put back in the priority queue. Multiple particles can occupy the same grid point at the same time. After a preset time (sampling time), an image is rendered by taking into account the imaging PSF. Bleaching is assumed to be instantaneous, taking into account the bleaching PSF. The probability $P(x, y)$ that a particle with coordinates (x, y) is bleached is given by

$$P(x, y) = \frac{k}{4}\left[\mathrm{erf}\left(\frac{x + L_x/2}{r_b/\sqrt{2}}\right) - \mathrm{erf}\left(\frac{x - L_x/2}{r_b/\sqrt{2}}\right)\right]$$
$$\times \left[\mathrm{erf}\left(\frac{y + L_y/2}{r_b/\sqrt{2}}\right) - \mathrm{erf}\left(\frac{y - L_y/2}{r_b/\sqrt{2}}\right)\right]. \qquad (21)$$

For each particle, a random number, uniformly distributed between 0 and 1, is generated. The particle is bleached if this number is smaller than $P(x, y)$.

Simulations of free diffusion are done with a diffusion coefficient of a typical order of magnitude for transmembrane proteins ($D = 0.25 \ \mu\mathrm{m}^2\,\mathrm{s}^{-1}$) and a mobile fraction ($M = 0.9$); simulations of anomalous diffusion are done with an anomalous exponent and transport factor that yield rather similar recovery curves within the time scale of the experiment ($\alpha = 0.75$, $K_\alpha = 0.3 \ \mu\mathrm{m}^2\,\mathrm{s}^{-\alpha}$), to provide a challenging case. The fixed jump length ($r_0 = 25$ nm) equals half the pixel size (50 nm). The bleached ROI measures 64×64 pixels ($k = 0.5$). The half width value at e^{-2} of the imaging PSF is chosen to be diffraction limited ($r_{\mathrm{im}} = 0.35 \ \mu\mathrm{m}$) and the width bleaching PSF is slightly larger ($r_b = 0.5 \ \mu\mathrm{m}$). An overview of the simulation parameters is given in Table 1. Each experiment has a concentration of about 3500 particles/$\mu\mathrm{m}^2$. With a sampling time $t_s = 0.4$ s, 10 prebleach images and 100 postbleach images are generated. The time between bleaching and the first postbleach image is the same as the time between any two subsequent images. Because CTRW is a nonstationary process[21] when $\alpha < 1$, all particles are given a new waiting time immediately after the bleaching procedure. The side of the square simulation area is six times larger than the side of the square-bleached ROI (Fig. 1). Particles that jump outside the simulation area are placed back at a random position on the edge of the simulation area. If the particle was bleached, it is then turned on again. The simulation program was written in C and ran on a high-performance cluster.

Table 1 Input parameters of the simulations.

Mesh size	$r_0 = 0.025 \ \mu\mathrm{m}$
Pixel size	$0.05 \ \mu\mathrm{m}$
Bleached ROI size (pixels)	64×64
Bleached ROI size (μm)	$3.2 \ \mu\mathrm{m} \times 3.2 \ \mu\mathrm{m}$
Bleaching psf (half width at e^{-2})	$r_b = 0.35 \ \mu\mathrm{m}$
Imaging psf (half width at e^{-2})	$r_{im} = 0.5 \ \mu\mathrm{m}$
Resolution parameter	$r^2 = 0.186 \ \mu\mathrm{m}^2$
Bleaching depth	$k = 0.5$
Mobile fraction (FDIM)	$M = 0.9$
Diffusion coefficient (FDIM)	$D = 0.25 \ \mu\mathrm{m}^2\,\mathrm{s}^{-1}$
Anomalous exponent (CTRW)	$\alpha = 0.75$
Transport factor (CTRW)	$K_\alpha = 0.3 \ \mu\mathrm{m}^2\,\mathrm{s}^{-\alpha}$
Sampling time	$t_s = 0.4$ s

4.2 Fitting Procedure

FRAP curves and intensity profiles are fitted by minimizing the reduced χ^2, i.e., the sum of squared differences between measured and fitted data, weighted by the inverse of the variance of each data point and divided by the degree of freedom, i.e., total number of data points minus the number of freely adjustable parameters. Before fitting, data are normalized with respect to the prebleach value. The variances of the data points in the recovery phase are determined by multiplying the variance of the prebleach data by the actual calculated value of the fitting function, and are therefore adjusted iteratively.

The freely adjustable parameters in the free diffusion model are the diffusion coefficient D, the mobile fraction M, and the bleaching depth k. The fitting according to TDDC or with the CTRW model is toward the transport factor K_α, or $K_\alpha*$, the anomalous exponent α, and the bleaching depth k.

When data are fitted with the CTRW model, the one-sided modified Levy function [Eq. (8)] has to be approximated. One hundred seventy terms are calculated, because the used precision (64 bits floating point) does not allow the evaluation of the gamma function for arguments larger than about 171. The integral in Eqs. (17) and (19) is numerically approximated by means of the trapezoidal rule. The integration parameter, s, is taken on a logarithmic grid. The values range from 2^{-20} to 10^7 with 16 points per octave. However, for large values of s, the series expansion in Eq. 8 does not always converge. This occurs when the exponential factor rises more rapidly than the gamma function for $n \leq 170$. It can be shown that for increasing s, the function first increases to its maximum and then monotonically decreases to zero. Hence, if during evaluation the function appears to increase for increasing s, after it has been decreasing, this is a sign that the series expansion is no longer converging. Therefore the function is only evaluated up to the previous value of s and approximated by 0 for all larger values. For two values of α ($\alpha = 1/2$, $\alpha = 1/3$), a closed expression exists for Eq. (8).

$$\alpha = 1/2 : A(s,t) = \frac{1}{\sqrt{\pi t}} \exp\left(-\frac{s^2}{4t}\right), \qquad (22)$$

$$\alpha = 1/3 : A(s,t) = \sqrt{\frac{s}{3t}}\left[I_{-1/3}\left(\frac{2s^{3/2}}{3\sqrt{3t}}\right) - I_{1/3}\left(\frac{2s^{3/2}}{3\sqrt{3t}}\right)\right], \qquad (23)$$

where $I_{-1/3}$ and $I_{1/3}$ are the modified Bessel functions. Comparison of the numerical evaluation of Eq. (17), respectively Eq. (19), with Eq. (8) for $\alpha = 1/2$, respectively $\alpha = 1/3$, confirmed the validity of the procedure. Fitting is done with an in-house developed Matlab (The Mathworks, Natick, Massachusetts) program.

4.3 Comparing Fits: the S-Score

We found that the reduced χ^2 is generally not conclusive to discriminate the various models and searched for a different criterion to quantify the goodness of fit. We present the S-score, a procedure inspired by the run-test.[33] While the χ^2 takes the absolute values of the residuals into account and ignores their sign, the S-score takes the succession of the signs in the autocorrelation function (ACF) of the residuals into account and ignores their value.

When the spatially integrated FRAP curve was fitted, the ACF of the residuals over time (t-ACF) was calculated. In case of randomly distributed residuals with little correlation, the autocorrelation will display many zero crossings.

When the spatial intensity profiles are fitted, the resulting residuals can be considered at each pixel in the image and for each time point. This allows the spatio-temporal autocorrelation functions (xyt-ACF) of the residuals to be calculated. Because the imaging PSF overlaps several pixels, there is correlation in the spatial distribution of the residuals at short distances, while the correlation at longer distances approaches zero. However, if the fit is not perfect, the central peak in the xyt-ACF can be broader than expected. For a three-dimensional ACF, it is not possible to simply count the number of zero crossings and a generalized procedure to quantitatively compare the goodness of fit is required.

We introduce the S-score in which the sign of each value of the ACF is compared to the sign of its nearest neighbors. The score is increased by 1 if both signs differ and the result is divided by the maximally obtainable score. Hence, in the case of the t-ACF, the S-score is given by

$$S = \frac{1}{N_t - 1} \sum_{k=1}^{N_t-1} \text{diffsign}\{G(kt_s), G[(k+1)t_s]\}, \qquad (24)$$

where "diffsign" is an operator that gives 0 if both arguments have the same sign and 1 otherwise. G is the t-ACF, t_s is the time between two subsequent data points, and N_t is the number of points in the t-ACF. Analogously, an expression that compares signs x-, y- and t- direction was derived for the xyt-ACF. Eventually a score between 0 (all values have the same sign) and 1 (all values have the opposite sign of their nearest neighbors) is obtained.

For the integrated FRAP curve, 100 data points are available and the first 50 points of the t-ACF are calculated. Analogously, the xyt-ACF is calculated over 50 points in time and 64 points in each spatial direction, since the fitted profile measures 128×128 pixels.

5 Results and Discussion

The simulations of free diffusion and anomalous diffusion are analyzed according to three models—FDIM, CTRW, and TDDC. It is expected that FDIM will give the best fit for the simulation of free diffusion and, similarly, CTRW for anomalous diffusion. TDDC can possibly lead to equally good fits in both cases. Two approaches will be applied to compare which has the better ability to distinguish the three different models: (a) integrated FRAP curves and (b) the time evolution of the intensity profile. To that purpose the function S [Eq. (24)] will be evaluated over 15 simulations for each parameter set (Table 1).

Initially, the resolution parameter, r, is kept fixed for both the integrated FRAP curves and the intensity profiles. This value is calculated from the input values for the bleaching and imaging PSF (Table 1). In a later stage it is investigated whether the prior knowledge of r is required to distinguish the different models. The intensity profiles are then fitted with a freely adjustable r. Based on previous work,[34] it is not expected that integrated curves based on single bleach ROI can be fitted with a freely adjustable r.

5.1 Fitting Spatially Integrated FRAP Curves

In this type of analysis the resolution parameter was kept fixed to the value used in the simulation. The results for free diffusion are listed in Table 2. The input values are quite well recovered by the fit according to FDIM. The corresponding FRAP curves together with the time sequence and the time autocorrelation of the weighted residuals are shown in Fig. 2. The residuals of the fit with CTRW and TDDC are almost identical and very similar to those according to FDIM.

Figure 2 and Table 3 give the results of the analyses of the simulations of anomalous diffusion. The residuals of the three models do not differ more than a few times their standard deviation. The input values are recovered well by the fit with CTRW. The fit with TDDC underestimates the anomalous exponent and the transport factor. The fit with FDIM mildly underestimates the bleaching depth.

The fit with CTRW appears to have a large risk of ending up in a local minimum. Several fits with different initial values have
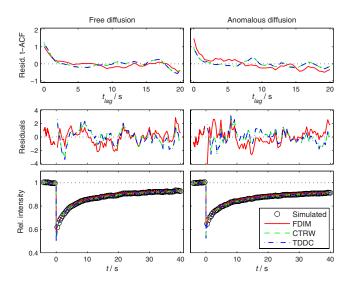
Table 2 Results of simulations of free diffusion. A 100-point recovery curve (40 s) was analyzed with fixed resolution parameter.

Model	$D/\mu m^2\,s^{-1}$ [a]	α or M [b]	k
Input	0.25	0.9	0.5
FDIM	0.26 ± 0.02 [c]	0.907 ± 0.007	0.493 ± 0.006
CTRW	0.6 ± 0.3	0.75 ± 0.07	0.6 ± 0.1
TDDC	0.32 ± 0.02	0.68 ± 0.02	0.60 ± 0.02

[a]In the case of CTRW or TDDC this column contains the transport factor, K_α, in $\mu m^2\,s^{-\alpha}$.
[b]α for CTRW and TDDC, M for FDIM.
[c]Uncertainties are reported by the standard deviations.

Fig. 2 Spatially integrated data of free (bottom left) and anomalous diffusion (bottom right) are fitted with the three different models and with fixed resolution parameter. The recovery curves resulting from the different models are not discernable on the scale of the figure. The corresponding weighted residuals and their t-ACF are shown, respectively, in the middle and on top. The traces corresponding to CTRW and TDDC are essentially superimposable.

Table 3 Results of simulations of anomalous diffusion. A 100-point recovery curve (40 s) was analyzed with fixed resolution parameter.

Model	$K_\alpha/\mu m^2\,s^{-\alpha}$ [a]	α or M [b]	k
Input	0.3	0.75	0.5
FDIM	0.18 ± 0.02 [c]	0.87 ± 0.02	0.430 ± 0.006
CTRW	0.31 ± 0.05	0.75 ± 0.03	0.50 ± 0.01
TDDC	0.24 ± 0.03	0.64 ± 0.04	0.53 ± 0.02

[a]In the case of FDIM this column contains the diffusion coefficient, D, in $\mu m^2\,s^{-1}$.
[b]α for CTRW and TDDC, M for FDIM.
[c]Uncertainties are reported by the standard deviations.

to be performed in order to find fit parameters that correspond to the global minimum. The fits with FDIM and TDDC, however, did not appear to be sensitive to the initial values.
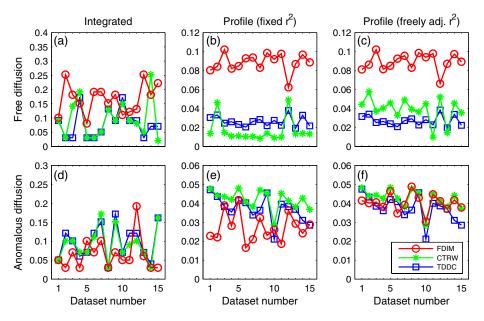
The scores S for the analyses with the different models fluctuate strongly over the different simulations, for both free diffusion [Fig. 3(a)] as well as anomalous diffusion [Fig. 3(d)]. In some cases the wrong model is suggested to be the most appropriate for the given dataset. For both free and anomalous diffusion, it can be concluded that there is no preference for a particular model.

Simulations of free and anomalous diffusions, where ROIs of different sizes are bleached, are both analyzed with the FDIM model. The apparent mobile fraction is expected to decrease for increasing ROI size and a constant observation time.[23] Figure 4 confirms this effect for the anomalous diffusion simulation. When free diffusion is simulated, the apparent mobile fraction hardly depends on the ROI size.

5.2 Fitting the Intensity Profile with Fixed Resolution Parameter

Figure 5 (top) shows the xyt-ACF of the residuals of the simulation of free diffusion for the various analyses. As the effect on the xyt-ACF is most pronounced at small lag-times, only the xyt-ACF of the residuals for the first 16 lag-times is shown. The corresponding recovered parameter values are given in Table 4. The xyt-ACF of the residuals of the analysis with CTRW shows a broadened peak for small lag-times that gradually decreases. This excludes CTRW from being the appropriate model for this dataset. The xyt-ACF for CTRW is very convincing. In case of TDDC, the effect is less pronounced, but nevertheless clearly visible. The S-scores are consistently higher for FDIM [Fig. 3(b)], clearly indicating that FDIM is the best model for this dataset. The parameter values obtained for FDIM are in good agreement with the input parameters.

Figure 5 (bottom) shows the xyt-ACF resulting from the analyses with the three models for the simulation of anomalous diffusion. The parameter values obtained with the various models are shown in Table 5. The S-scores are consistently higher for the analysis with CTRW than for the analysis with FDIM [Fig. 3(e)]. The scores for the analysis with TDDC fluctuate between the values for the other models, sometimes closely approaching the score for CTRW. For the example, in Fig. 3, the difference between CTRW and TDDC is not clear. As for the simulation of free diffusion, the results for the simulation of anomalous diffusion obtained with the proper analysis
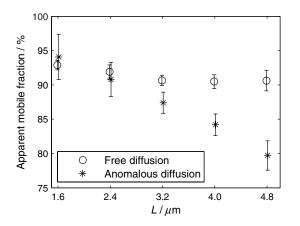
Fig. 3 Overview of the S scores belonging to the simulations of free [(a), (b), (c)] and anomalous [(d), (e), (f)] diffusion. In (a) and (d) the integrated FRAP curves are fitted. The S-scores for the fits of the intensity profile are shown in (b) and (e) for a fixed resolution parameter and in (c) and (f) for a freely adjustable resolution parameter.

model are somewhat better in agreement with the input parameters than for the spatially integrated case. The analysis with TDDC recovers an anomalous exponent that is in quite good agreement with the input value, although the transport factor is significantly underestimated.

In contrast to the integrated approach, the fit with CTRW is less sensitive to the initial values. The results of a fit with TDDC, which takes negligible time with respect to a fit with CTRW, are used as initial values and this always leads to the global minimum in the least-squares fitting.

5.3 Fitting the Intensity Profile with Freely Adjustable Resolution Parameter

The effective resolution parameter r is generally unknown in an FRAP experiment because the effective bleach resolution r_b

Fig. 4 Simulations of free and anomalous diffusion analyzed with FDIM by integrating over the ROI. In the case of anomalous diffusion, the apparent mobile fraction depends on the size ($L \times L$, where $L = L_x = L_y$) of the bleached ROI, while this is not the case for free diffusion. Each data point is the average of 15 repetitions; the error bars indicate the standard deviation. Resolution parameter was kept fixed.
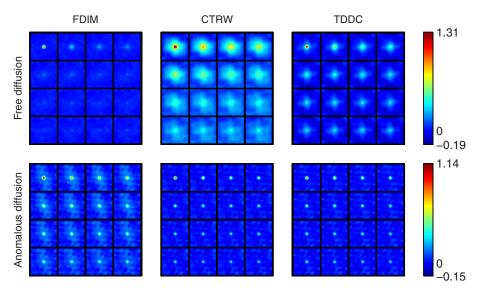
depends on many conditions.[35] It was demonstrated by Deschout et al.[31] that the effective resolution r can be included as a free fitting parameter when using the full tempo-spatial profile of the rFRAP method. As a next step in this study, we have investigated the effect of having r as a free fitting parameter on the retrieved diffusion parameters. The results for the simulation of free diffusion are given in Table 6. The results of the simulation of anomalous diffusion can be found in Table 7. For both cases the diffusion coefficient and mobile fraction (FDIM) or the transport factor and anomalous exponent (CTRW) as well as the bleaching depth are in agreement with the input parameter and as good as in the analyses when the resolution parameter was kept fixed to the input value. The resolution parameter is reasonably well recovered when taking into account the standard deviations of the resulting values.

The scores for the fit of free diffusion with each model are given in Fig. 3(c). In this case FDIM consequently gets the highest score over all simulations, as was the case with the fixed resolution parameter. However, the scores for the fit of the simulation of anomalous diffusion [Fig. 3(f)] indicate that it is less obvious to obtain consistent results regarding the most applicable model over all datasets.

As compared to the analysis with fixed resolution parameter, the anomalous exponent in the simulation of anomalous diffusion is more underestimated by TDDC analysis, while the transport factor is equally underestimated.

5.4 Discussion

FRAP simulations of free and anomalous diffusions were analyzed according to two different approaches. The first is the classic FRAP approach based on the analysis of the time sequence of the intensities resulting from the integration over the bleached ROI. Because of the integration, the spatial information is discarded and only the temporal evolution remains. The second approach, rFRAP, retains the spatial information by considering the intensity profile over an area larger than the bleached ROI, and this at various time points. The aim of this work was to

Fig. 5 Simulations of free and anomalous diffusion were analyzed with three different models and with fixed resolution parameter. Each small square panel represents the spatial autocorrelation function of the residuals for a certain lag-time when fitting the intensity profile. The sequence of the small panels shows the evolution of the spatial autocorrelation functions as function of lag-time for the first 16 lag-times. The lag-time evolves from left to right and from top to bottom. The bar at the right displays the color code for the values of the autocorrelation function.

explore the capabilities of rFRAP approaches to unambiguously distinguish between three different models—FDIM, CTRW, and TDDC. FDIM and CTRW are fundamental models because of their physical justification. TDDC offers a rather phenomenological model for anomalous diffusion. The simulation parameters are chosen so that the various models yield a challenging case for discrimination. In order to compare the goodness of fit of the different models, we suggested the S-score that favors many fluctuations around zero in the ACF. It was found that fitting the intensity profile has a higher power to discriminate between different models of diffusion. This was especially the case for simulations of free diffusion, where the correct model (FDIM) resulted in a consistently better fit. In the case of simulations of anomalous diffusion, where the correct model is CTRW, this effect remains but is less pronounced.

When integrated FRAP curves are analyzed, the residuals and their temporal ACF are not indicative toward a particular model within an experimentally feasible time interval, as the S-scores are not indicative [Fig. 3(a) and 3(d)]. This is in agreement with the conclusion of Feder et al.,[17] stating that an

unambiguous distinction between FDIM and TDDC cannot be deducted from a single FRAP curve on a moderate time scale.

If the resolution parameter is freely adjustable, the effect on the S-scores is less pronounced and it becomes virtually impossible to indicate the best model for the simulation of anomalous diffusion.

Least-squares analyses with the CTRW model appear to have the risk of arriving at a local minimum. We find that this can be circumvented in the intensity profile approach by using as initial values the parameters resulting from a fit with TDDC. The fit with TDDC takes a negligible time as compared to the fit with CTRW. When integrated FRAP curves are fitted, different sets of initial values have to be used to assure the global minimum.

The recovered parameters are in very good agreement with the input parameters of the simulation provided that the analysis is done with the correct model and the resolution parameter is fixed. If the resolution parameter is freely adjustable, the parameters of the diffusion model are essentially recovered.

In the integrated FRAP approach, the analysis with TDDC of the simulation of anomalous diffusion by means of CTRW

Table 4 Results of simulations of free diffusion. The intensity profile in 100 recovery images (40 s) was analyzed with fixed resolution parameter.

Model	$D/\mu m^2\ s^{-1}$ [a]	α or M [b]	k
Input	0.25	0.9	0.5
FDIM	0.25 ± 0.01 [c]	0.898 ± 0.006	0.499 ± 0.005
CTRW	1.0 ± 0.3	0.6 ± 0.1	0.55 ± 0.03
TDDC	0.170 ± 0.006	0.94 ± 0.03	0.456 ± 0.007

[a]In the case of CTRW or TDDC this column contains the transport factor, K_α, in $\mu m^2\ s^{-\alpha}$.
[b]α for CTRW and TDDC, M for FDIM.
[c]Uncertainties are reported by the standard deviations.

Table 5 Results of simulations of anomalous diffusion. The intensity profile in 100 recovery images (40 s) was analyzed with fixed resolution parameter.

Model	$K_\alpha/\mu m^2\ s^{-\alpha}$ [a]	α or M [b]	k
Input	0.3	0.75	0.5
FDIM	0.13 ± 0.01 [c]	0.94 ± 0.01	0.448 ± 0.008
CTRW	0.30 ± 0.04	0.75 ± 0.03	0.50 ± 0.02
TDDC	0.17 ± 0.02	0.74 ± 0.04	0.46 ± 0.02

[a]In the case of FDIM this column contains the diffusion coefficient, D, in $\mu m^2\ s^{-1}$.
[b]α for CTRW and TDDC, M for FDIM.
[c]Uncertainties are reported by the standard deviations.

Table 6 Results of simulations of free diffusion. The intensity profile in 100 recovery images (40 s) was analyzed with freely adjustable resolution parameter.

Model	$D/\mu m^2\,s^{-1\,a}$	α or M^b	k	$r^2/\mu m^2$
Input	0.25	0.9	0.5	0.186
FDIM	0.25 ± 0.01^c	0.897 ± 0.005	0.501 ± 0.006	0.21 ± 0.04
CTRW	0.4 ± 0.3	0.8 ± 0.1	0.49 ± 0.02	0.002 ± 0.008
TDDC	0.185 ± 0.006	0.90 ± 0.03	0.454 ± 0.007	0.002 ± 0.006

[a] In the case of CTRW or TDDC this column contains the transport factor, K_α, in $\mu m^2\,s^{-\alpha}$
[b] α for CTRW and TDDC, M for FDIM.
[c] Uncertainties are reported by the standard deviations.

Table 7 Results of simulations of anomalous diffusion. The intensity profile in 100 recovery images (40 s) was analyzed with freely adjustable resolution parameter.

Model	$K_\alpha/\mu m^2\,s^{-\alpha\,a}$	α or M^b	k	$r^2/\mu m^2$
Input	0.3	0.75	0.5	0.186
FDIM	0.14 ± 0.01^c	0.90 ± 0.02	0.49 ± 0.01	1.0 ± 0.2
CTRW	0.31 ± 0.03	0.75 ± 0.02	0.50 ± 0.02	0.1 ± 0.1
TDDC	0.18 ± 0.02	0.71 ± 0.04	0.46 ± 0.02	0.02 ± 0.04

[a] In the case of FDIM this column contains the diffusion coefficient, D, in $\mu m^2\,s^{-1}$.
[b] α for CTRW and TDDC, M for FDIM.
[c] Uncertainties are reported by the standard deviations.

yields an anomalous exponent and transport factor that are underestimated compared to the input value. When the intensity profiles are fitted, either with a fixed or freely adjustable resolution parameter, the anomalous exponent is more precisely retrieved with TDDC while the transport factor is even more underestimated.

6 Conclusion

It has been shown that fitting the intensity distribution over an area larger than the bleached area during recovery is capable of distinguishing different models of diffusion to a given dataset. Only a single experiment over a rather restricted time window is required. It can be expected that this approach is of utmost importance when experiments have to be performed on living cells.

References

1. D. M. Owen et al., "Quantitative microscopy: protein dynamics and membrane organisation," *Traffic* **10**(8), 962–971 (2009).
2. P.-F. Lenne and A. Nicolas, "Physics puzzles on membrane domains posed by cell biology," *Soft Matter* **5**(15), 2841–2848 (2009).
3. P.-F. Lenne et al., "Dynamic molecular confinement in the plasma membrane by microdomains and the cytoskeleton meshwork," *EMBO J.* **25**(14), 3245–3256 (2006).
4. K. Ritchie et al., "The fence and picket structure of the plasma membrane of live cells as revealed by single molecule techniques," *Mol. Membr. Biol.* **20**(1), 13–18 (2003).
5. E. Barkai, Y. Garini, and R. Metzler, "Strange kinetics of single molecules in living cells," *Phys. Today* **65**(8), 29–35 (2012).
6. K. Notelaers et al., "Ensemble and single particle fluorimetric techniques in concerted action to study the diffusion and aggregation of the glycine receptor α3 isoforms in the cell plasma membrane," *BBA-Biomembranes* **1818**(12), 3131–3140 (2012).
7. M. A. Digman et al., "Measuring fast dynamics in solutions and cells with a laser scanning microscope," *Biophys. J.* **89**(2), 1317–1327 (2005).
8. M. Saxton and K. Jacobson, "Single-particle tracking: applications to membrane dynamics," *Ann. Rev. Bioph. Biom.* **26**(1), 373–399 (1997).
9. Z. Petrasek and P. Schwille, "Fluctuations as a source of information in fluorescence microscopy," *J. Roy. Soc. Interface* **6**(Suppl. 1), S15–S25 (2009).
10. D. Axelrod et al., "Mobility measurement by analysis of fluorescence photobleaching recovery kinetics," *Biophys. J.* **16**(9), 1055–1069 (1976).
11. D. M. Soumpasis, "Theoretical analysis of fluorescence photobleaching recovery experiments," *Biophys. J.* **41**(1), 95–97 (1983).
12. C.-L. Wey, R. A. Cone, and M. A. Edidin, "Lateral diffusion of rhodopsin in photoreceptor cells measured by fluorescence photobleaching and recovery," *Biophys. J.* **33**(2), 225–232 (1981).
13. Y. G. Anissimov et al., "Fluorescence recovery after photo-bleaching as a method to determine local diffusion coefficient in the stratum corneum," *Int. J. Pharm.* **435**(1), 93–97 (2012).
14. J. Hagman, N. Loren, and A. M. Hermansson, "Probe diffusion in kappa-carrageenan gels determined by fluorescence recovery after photobleaching," *Food Hydrocolloid.* **29**(1), 106–115 (2012).
15. F. Cardarelli et al., "Fluorescent recovery after photobleaching (FRAP) analysis of nuclear export rates identifies intrinsic features of nucleocytoplasmic transport," *J. Biol. Chem.* **287**(8), 5554–5561 (2012).
16. M. Kang and A. K. Kenworthy, "Complex applications of simple FRAP on membranes," in *Biomembrane Frontiers, Handbook of Modern Biophysics*, pp. 187–221, Humana Press, New York, NY (2009).
17. T. Feder et al., "Constrained diffusion or immobile fraction on cell surfaces: a new interpretation," *Biophys. J.* **70**(6), 2767–2773 (1996).
18. J. Wu and K. M. Berland, "Propagators and time-dependent diffusion coefficients for anomalous diffusion," *Biophys. J.* **95**(4), 2049–2052 (2008).
19. R. Metzler and J. Klafter, "The random walk's guide to anomalous diffusion: a fractional dynamics approach," *Phys. Rep.* **339**(1), 1–77 (2000).

20. M. J. Saxton, "Anomalous subdiffusion in fluorescence photobleaching recovery: a Monte Carlo study," *Biophys. J.* **81**(4), 2226–2240 (2001).
21. A. Lubelski and J. Klafter, "Fluorescence recovery after photobleaching: the case of anomalous diffusion," *Biophys. J.* **94**(12), 4646–4653 (2008).
22. J. F. Nagle, "Long tail kinetics in biophysics?," *Biophys. J.* **63**(2), 366–370 (1992).
23. L. Salomé et al., "Characterization of membrane domains by FRAP experiments at variable observation areas," *Eur. Biophys. J.* **27**(4), 391–402 (1998).
24. E. Yechiel and M. A. Edidin, "Micrometer-scale domains in fibroblast plasma membranes," *J. Cell Biol.* **105**(2), 755–760 (1987).
25. Q. Tang and M. Edidin, "Lowering the barriers to random walks on the cell surface," *Biophys. J.* **84**(1), 400–407 (2003).
26. K. Braeckmans et al., "Three-dimensional fluorescence recovery after photobleaching with the confocal scanning laser microscope," *Biophys. J.* **85**(4), 2240–2252 (2003).
27. D. Mazza et al., "A new FRAP/FRAPa method for three-dimensional diffusion measurements based on multiphoton excitation microscopy," *Biophys. J.* **95**(7), 3457–3469 (2008).
28. E. A. Schnell et al., "Diffusion measured by fluorescence recovery after photobleaching based on multiphoton excitation laser scanning microscopy," *J. Biomed. Opt.* **13**(6), 064037 (2008).
29. O. Dushek and D. Coombs, "Improving parameter estimation for cell surface FRAP data," *J. Biochem. Bioph. Methods* **70**(6), 1224–1231 (2008).
30. P. Wedekind et al., "Line-scanning microphotolysis for diffraction-limited measurements of lateral diffusion," *Biophys. J.* **71**(3), 1621–1632 (1996).
31. H. Deschout et al., "Straightforward FRAP for quantitative diffusion measurements with a laser scanning microscope," *Opt. Express* **18**(22), 22886–22905 (2010).
32. M. Kang, E. Di Benedetto, and A. Kenworthy, "Proposed correction to Feder's anomalous diffusion FRAP equations," *Biophys. J.* **100**(3), 791–792 (2011).
33. H. Toutenburg, "Draper N., H. Smith, Applied Regression Analysis, John Wiley & Sons, New York (1966). 407 S., 43 Abb., 2 Tab., 180 Literaturangaben, Preis: s 90," *Biometrische Zeitschrift* **11**(6), 427–427 (1969).
34. N. Smisdom et al., "Fluorescence recovery after photobleaching on the confocal laser-scanning microscope: generalized model without restriction on the size of the photobleached disk," *J. Biomed. Opt.* **16**(4), 046021 (2011).
35. K. Braeckmans et al., "Anomalous photobleaching in fluorescence recovery after photobleaching measurements due to excitation saturation—a case study for fluorescein," *J. Biomed. Opt.* **11**(4), 044013 (2006).